2000

Interannual Climate Variability in the Central Andes and Its Relation to Tropical Pacific and Atlantic Forcing

M. Vuille
Raymond S Bradley, *University of Massachusetts - Amherst*
F. T Keimig

JOURNAL OF GEOPHYSICAL RESEARCH, VOL. 105, NO. D10, PAGES 12,447-12,460, MAY 27, 2000

Interannual climate variability in the Central Andes and its relation to tropical Pacific and Atlantic forcing

Mathias Vuille, Raymond S. Bradley and Frank Keimig

Climate System Research Center, Department of Geosciences, University of Massachusetts, Amherst

Abstract. The main spatiotemporal modes of interannual temperature and austral summer (DJF) precipitation variability in the Central Andes are identified based on a two-way principal component analysis (PCA) of 30-year (1961-1990) monthly station data and related to contemporaneous tropical Pacific and Atlantic sea surface temperature anomalies (SSTAs). In addition, various meteorological fields, based on National Centers for Environmental Prediction / National Center for Atmospheric Research (NCEP/NCAR) reanalysis, NOAA-Outgoing Longwave Radiation (OLR) and station data, are analyzed during periods of strong positive and negative SSTA and the respective composites tested for local significance using a Student's *t*-test approach. Temperature variability in the Central Andes is primarily related to El Niño - Southern Oscillation (ENSO) and closely follows SSTA in the central equatorial Pacific with a lag of 1-2 months. In the southern Altiplano, temperatures have significantly increased since the late 1970s. DJF precipitation is also primarily related to ENSO, featuring below (above) average precipitation during El Niño (La Niña). Precipitation over the dry western part of the Altiplano shows the closest relationship with ENSO, due to ENSO-induced atmospheric circulation anomalies. Precipitation variability over the western Altiplano features a decadal-scale oscillation, related to a similar climatic shift in the tropical Pacific domain in the late 1970s. Over the northern Altiplano the precipitation signal is reversed in the austral summer following the peak phase of ENSO, presumably due to the temporal evolution of tropical Pacific SSTA, rapidly switching from one state to the other. No evidence for a tropical Atlantic influence on DJF precipitation was found. SSTAs in the tropical NE Atlantic, however, presumably are influenced by heating and convection over the Altiplano through an upper air monsoon return flow, altering the strength of the NE trades that emanate from the Sahara High.

1. Introduction

Several studies have recently provided new information on local and large-scale atmospheric conditions associated with summer precipitation variability in the Central Andes and the interandean plateau (the Altiplano). While *Hardy et al.* [1998] presented a local record of the daily and annual meteorological cycle at high altitude, *Vuille et al.* [1998], *Garreaud* [1999], and *Lenters and Cook* [1999] focused on the regional- to large-scale mechanisms associated with precipitation during austral summer, and *Vuille* [1999] showed how interannual precipitation variability is related to atmospheric circulation anomalies during extreme phases of the Southern Oscillation (SO). However, these studies fall short in explaining the spatial precipitation variability over the Altiplano itself, because they are either based on data from only one part of the Altiplano or they consider the entire region as an entity, which is inappropriate, given the extreme spatial and temporal variability of precipitation on the Altiplano [*Vuille et al.*, 1998]. In this study we therefore analyze the spatiotemporal behavior of austral summer (DJF) precipitation and monthly temperature anomalies based on a dense station network, covering the entire Altiplano, which allows us to resolve the aforementioned spatial variability. In addition, the influence of tropical Pacific and Atlantic sea surface temperature anomalies (SSTA) upon precipitation and temperature variability in the different parts of the Altiplano is examined.

The Altiplano extends along the central portion of the Andes as a high intramontane plateau with an average elevation of 3700-4400 m (650-600 hPa) from about 14°S-22°S (Figure1). Here the Andes split up into an eastern and a western cordillera, which effectively separates the low-level flow to the east and the west (Figure 2a). While the Southeast Pacific Anticyclone in combination with cold SSTs produces dry and stable conditions to the west, with moist air trapped below the subsidence inversion at about 900 hPa, a thermal heat low develops to the east during summer months, and the lower troposphere is characterized by warm and humid conditions. The Altiplano separating these two opposite climatic conditions is accordingly characterized by a very strong climatic gradient with average annual precipitation amounts below 200 mm yr^{-1} in the southwestern part and more than 800 mm yr^{-1} in the northeastern. Most of the precipitation in the Central Andes (50-80% of the annual rainfall amount, see Figure 1) falls during the austral summer months DJF, associated with the development of convective cloudiness over the Central Andes and the southwestern part of the Amazon (Figure 2b). Winter precipitation is not a very frequent phenomena, and the recorded precipitation amounts are low [*Vuille and Ammann*, 1997; *Hardy et al.*, 1998]. During the summer months however, intense solar heating of the Altiplano surface leads to a destabilization of the boundary layer, inducing deep convection and moist air advection from the eastern interior of the continent [*Vuille et al.*, 1998; *Garreaud*, 1999]. This moist air is usually released in typical afternoon and evening showers over the Altiplano

Paper number 2000JD900134
0148-0227/00/2000JD900134$09.00

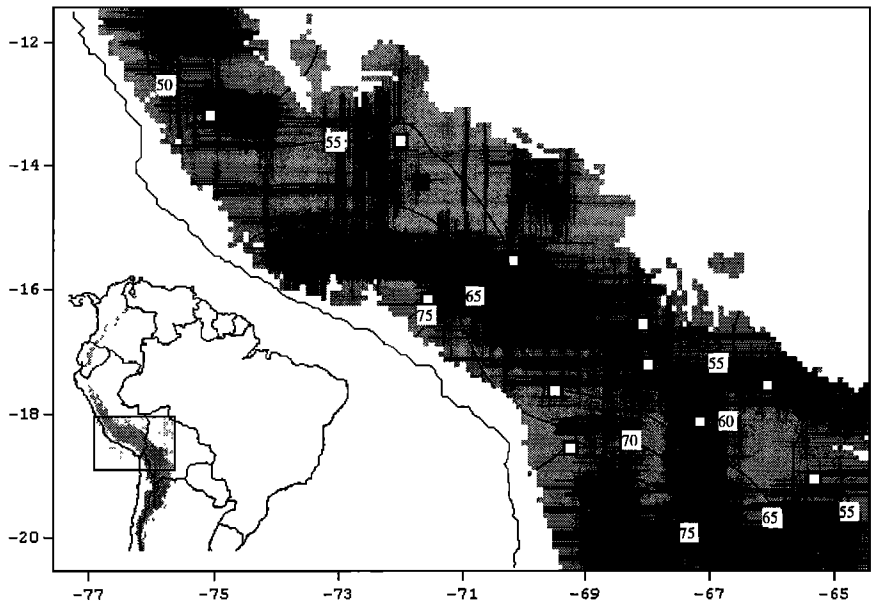

Figure 1. Location of the stations with precipitation and temperature records in the Central Andes which were used in this study. Open squares indicate stations with precipitation and temperature data; solid squares denote stations that only include precipitation data. Shaded areas show elevations > 1500 m. Contour lines indicate relative contribution of DJF precipitation to annual precipitation total (in %). Contour interval is 5%. Location of the Central Andes is shown in the bottom left.

[*Garreaud and Wallace*, 1997]. Nonetheless, precipitation events can only occur during periods of favorable upper air conditions, with prevailing easterly winds or with upper air divergence, which favor near-surface moisture influx from the east and sustain deep convection over the Altiplano [*Jacobeit*, 1992; *Garreaud*, 1999]. Therefore the temporal evolution of summer precipitation on the Altiplano has a very distinct pattern with week-long dry periods interrupted by rainy events of similar length. In the upper troposphere an anticyclonic vortex, the Bolivian High, develops during the summer months (see Figure 2b). A variety of modeling studies have provided evidence that this high-pressure system is a transient feature related to latent heat release over the Amazon Basin, rather than a local response to diabatic heating over the Altiplano itself [e.g., *Silva Dias et al.*, 1983; *Lenters and*

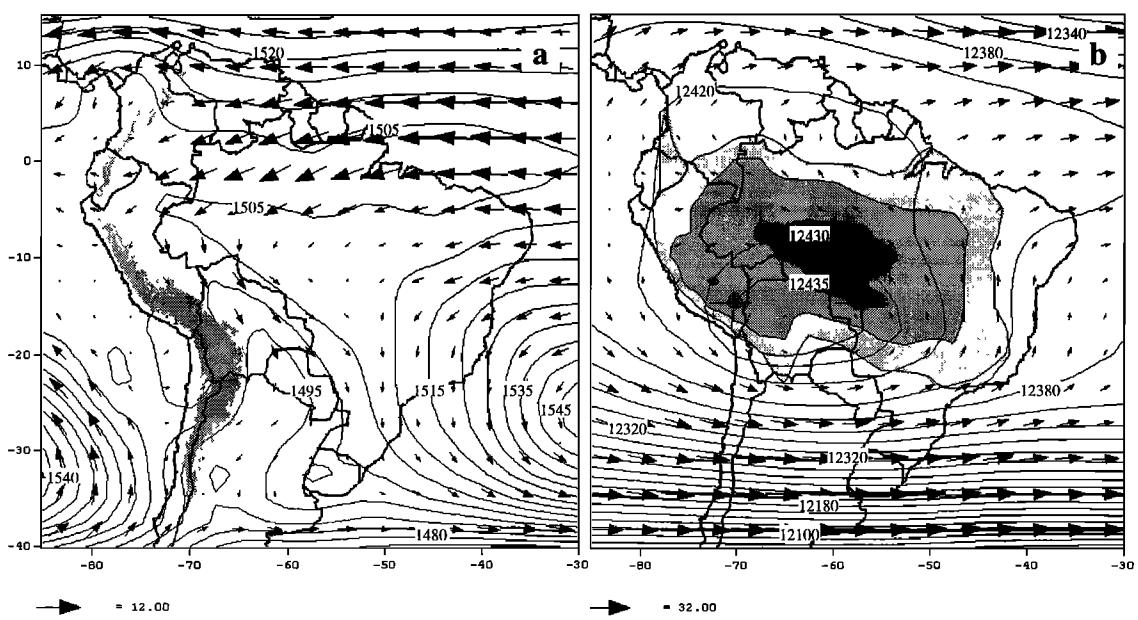

Figure 2. Austral summer (DJF) climatological mean (1968-1996) based on NCEP/NCAR reanalysis data for (a) 850 hPa winds and geopotential height. Contour interval is 5 gpm, shaded area represents elevation above 3000 m. (b) 200 hPa winds and geopotential height. Contour interval is 20 gpm, 10 gpm above 12,420 and 5 gpm above 12,430. Superimposed is mean DJF NOAA-OLR (1974-1998) with light, medium, and dark shading indicating values less than 225, 210 and 195 W m^{-2}.

Cook, 1997]. The positioning and the strength of the Bolivian High is intrinsically linked to precipitation anomalies over the Altiplano [*Aceituno and Montecinos*, 1993; *Vuille et al.*, 1998; *Lenters and Cook*, 1999; *Vuille*, 1999]. During austral summer precipitation events on the Altiplano an intensification and southward displacement of this high-pressure system can be observed. On the other hand, a weakened and northward displaced Bolivian High is usually associated with the week-long dry periods on the Altiplano, a pattern that can also be observed on interannual timescales [*Vuille*, 1999].

Several authors have reported on the relationship between interannual variability of summer precipitation in the Central Andes and the El Niño-Southern Oscillation (ENSO) phenomenon [e.g., *Thompson et al.*, 1984; *Aceituno*, 1988; *Ronchail*, 1995; *Vuille*, 1999]. A common finding of all these studies is the tendency toward increased air temperatures and below average summer precipitation during El Niño events. According to *Ronchail* [1995] the ENSO influence on precipitation is particularly strong very early (October) and toward the end of the rainy season (February). The statistical significance of all these results, however, is quite variable and often rather weak. Since the main moisture source for precipitation over the Altiplano is the tropical lowlands to the east of the Andes, and ultimately over the trade wind regions of the tropical Atlantic (see Figure 2a), a closer examination of the relation with tropical Atlantic SSTA seems appropriate [see *Enfield*, 1996; *Zhou and Lau*, 1998; *Vuille et al.*, 2000].

In section 2 we present the station data (monthly precipitation and temperature) and the gridded data sets (GISST-SST, NOAA-OLR, and NCEP/NCAR reanalysis), upon which this study is based. We then describe the methods (principal component analysis (PCA) and composite analysis) which were applied in this study. Section 3 presents the results from the PCA, applied to the tropical Pacific and Atlantic SSTA data. Section 4 presents the results from the PCA and composite analysis applied to monthly temperature anomalies, while section 5 presents the same results for austral summer precipitation (DJF). Section 6 contains a discussion of the most interesting new results, and section 7 summarizes this study and concludes with some final remarks.

2. Data and Methods

Monthly mean SST data on a 1° latitude × 1° longitude grid were obtained from the Global sea-Ice and Sea Surface Temperature (GISST) data set version 2.3a (Hadley Center, Meteorological Office, Bracknell, England). The original data were resampled into 2° × 2° grid cells, smoothed using a Hamming weights low-pass filter with a notch at $f = 4$ cycles/yr, thereby removing fluctuations with periods of less than 3 months [see *Stearns and David*, 1988], and monthly anomalies were computed over the tropical Pacific (30°N-40°S, 160°E - 80°W) and Atlantic (30°N-40°S, 80°W-10°E) by subtracting the mean monthly values for the period 1961-1990.

Monthly Outgoing Longwave Radiation (OLR) data with a 2.5° latitude × 2.5° longitude grid were obtained from the NOAA interpolated data set [*Liebmann and Smith*, 1996] for the period June 1974 to December 1990 (with some months in 1978 missing) and used as a proxy of tropical convection and precipitation [see *Horel et al.*, 1989; *Kousky and Kayano*, 1994]. To describe the large-scale atmospheric structure and circulation associated with extreme phases of the main SSTA modes, we used monthly gridded 200 hPa wind and geopotential height and 600 hPa temperature data, extracted from the National Centers for Environmental Prediction / National Center for Atmospheric Research (NCEP/NCAR) reanalyzed meteorological fields for the period 1961-1990. A detailed description of this data set can be found in *Kalnay et al.* [1996].

Monthly precipitation and monthly mean temperature station data cover the entire Altiplano and the adjacent part of the southern Peruvian Andes between ~2500 m and ~5250 m from 11.5°S to 20.5°S (see Figure 1). All stations (except Chacaltaya, Bolivia, which is maintained by the University Major de San Andrés in La Paz) form part of the national meteorological networks (Dirección General de Aguas, Chile; Servicio Nacional de Meteorología e Hidrología in Perú and Bolivia). Additional data were obtained from the Global Historical Climatology Network (GHCN). From this original data set of 228 precipitation and 50 temperature stations, a subset of 31 (11) precipitation (temperature) stations was selected, equally distributed along the Andean range and each at least 80% complete in the time period analyzed, 1961-1990. We used a regularly spaced station network to avoid problems associated with computing PCs for irregularly spaced data [*Karl et al.*, 1982]. The temperature network is less dense and, because of the limited number of available stations, covers a smaller area (13°S-19°S) than the precipitation data (11.5°S-20.5°S). Nonetheless, this network is considered sufficient, as temperature shows less spatial variability than precipitation. All data were error-checked and, if necessary, homogenized using double-cumulative techniques. Cross correlations between all stations were computed, and missing data periods were filled using linear regression with stations showing the highest correlation, always significant at the 99% level. Since the rainy season is limited to austral summer (DJF), analysis of precipitation variability was carried out for this season only on the basis of 3-monthly sums. Figure 1 shows that the southwestern part of the Altiplano receives precipitation almost exclusively during this time of the year (>75% of the annual amount), while in the northeast, the rainy season starts earlier and lasts into March and April (reducing the contribution of DJF to ~50%). All DJF sums were transformed into γ-probabilities because of its distinctly asymmetric distribution, skewed to the right and bounded by zero. After the transformation the data ranged from zero (no precipitation) to 0.99 in the year of maximum precipitation. Temperature data were smoothed in the same way as the SST data, and monthly anomalies were computed by subtracting the mean monthly values for the period 1961-1990. Temperature analysis was performed on the entire continuous record.

To extract the main modes of variability, a rotated PCA was performed in the S-mode (spatial) sense, based on the interstation correlation matrix of both the precipitation and temperature data sets. Rotation of the PCs was based on the Varimax criterion and applied, because rotated PCs (VPCs) usually yield spatial loading patterns that are more representative of the real modes of variability, especially beyond the first PC [e.g., *Richman and Lamb*, 1985; *Richman*, 1986]. However, the fact that the number of UPCs retained for subsequent rotation significantly affects the rotated solution remains a drawback of rotation. Therefore several tests were applied to determine the number of UPCs that contain a nonrandom signal [*North et al.*, 1982; *Overland and Preisendorfer*, 1982]. To plot the spatial loading patterns associated with each PC, data were interpolated between the stations using spherical kriging.

In a next step the resulting time series (factor scores) of the PCs were cross-correlated with Pacific and Atlantic SSTA. Contemporaneous and lagged correlations were carried out to detect if

an ENSO signal might be delayed due to a transfer of the signal through the tropical North Atlantic [*Enfield and Mayer*, 1997]. All correlation significance levels account for serial correlation in the data by an adjustment in the degrees of freedom [see *Davis*, 1976]. As a result, spatial patterns emerged over the tropical Pacific and Atlantic, potentially related to a certain mode of temperature or precipitation variability over the Central Andes. However, such pixel-based cross correlations of time series carry the danger that statistically significant but physically meaningless correlations emerge in areas that have no physical connection to this part of the Andes. To confirm the results, we therefore performed the reverse procedure. Again, we extracted the PCs, this time from the monthly SSTA in the tropical Pacific (30°N-40°S, 160°E-80°W) and Atlantic (30°N-40°S, 80°W-10°E). This PCA was done separately for the two basins, which allowed us to identify whether regional patterns of precipitation or temperature anomalies relate to the Pacific or the Atlantic. The first unrotated PC (PAC-UPC1, ATL-UPC1) was considered to have potential physical meaning [see *Montroy*, 1998] and retained in the analysis. The score time series of the first unrotated and all Varimax rotated PCs, representing the main modes of tropical SST variability, were then cross-correlated with the station data from the Altiplano (DJF γ-precipitation and monthly temperature anomalies). Coherency maps of cross correlations between temperature or precipitation and tropical SSTA modes were plotted, again tested for significance, and the results of this second approach were compared to the patterns obtained previously from the first analysis to see whether they compared favorably.

Finally, composites of station data and of various meteorological fields over the South American continent were analyzed during the six strongest periods (DJF) of positive (WARM) and negative (COLD) SSTA of the respective oceanic modes to confirm the proposed relationships and to gain a better understanding of the mechanisms involved with precipitation and temperature anomalies over the Altiplano region. OLR, 200 hPa wind, and geopotential height DJF composites during COLD and WARM were tested for local significance using a Student's *t*-test. Composites of Altiplano station temperature and 600 hPa (~ Altiplano surface level) air temperature are independent of the season and based on periods when the averaged standardized score time series of the respective SSTA mode is >1 (WARM) and <-1 (COLD). In addition, air temperature composites account for the apparent 2-month lag between SSTA peak and temperature signal over the Altiplano (see section 4).

3. Modes of Tropical Pacific and Atlantic SST Variability

The basic statistics of the PCA performed on the SSTA in the Atlantic and Pacific are shown in Table 1, and the spatial loading patterns and the score time series (Pacific only) of UPC1 and VPC1-2 are shown in Figure 3. In both the Atlantic and the Pacific analyses the first six PCs were considered to contain a nonrandom signal [*North et al.*, 1982] and therefore retained and rotated using the Varimax criterion.

A clear ENSO signal emerges from the PCA of tropical Pacific SSTA, which is no surprise since SST variability on interannual timescales in the tropical Pacific domain is largely controlled by this phenomenon. Both PAC-UPC1 and PAC-VPC1 show the typical ENSO characteristics in both their spatial pattern (Figures 3a-3b) and their temporal evolution (Figures 3d-3e), featuring the typical broad tongue centered on the equator and extending westward beyond the dateline, and negative loadings that extend from west of 160°E at the equator in a *V*-shape fashion to 30°N and 30°S. While PAC-UPC1 is more representative of SSTA in the central equatorial Pacific (highest correlation with NINO4, $r = 0.85$), PAC-VPC1 is the dominant mode in the eastern part of the basin (highest correlation with NINO3, $r = 0.91$). All major El Niño and La Niña periods in the time interval 1961-1990 are represented as high (El Niño) and low (La Niña) score values in both time series (indicated with E and L in Figures 3d-3e). Also evident in Figure 3d is a shift in the climatic regime of the Pacific starting in the late 1970s, with a tendency toward more frequent El Niño and fewer La Niña events [see *Ebbesmeyer et al.*, 1991]. The spatial loading pattern of PAC-VPC2 represents SST variability on the poleward flanks of the climatological Innertropical Convergence Zone (ITCZ). It is a precursor mode to PAC-VPC1, with SSTA around 10°-30°N peaking several months prior to ENSO [see *Tourre and White*, 1995]. PAC-VPC3-6 (not shown) are not primarily related to ENSO and showed no clear relationship with climatic variability on the Altiplano in the latter analysis. They were therefore not used any further in this study.

The spatial loading patterns of ATL-UPC1 and ATL-VPC1-2 are shown in Figures 3g-3i. While ATL-UPC1 has its highest fraction of explained variance spread over almost the entire tropical Atlantic, the rotated solution shows a better resolved picture with most of the explained variance within the trade wind regions of the tropical North and South Atlantic, respectively (ATL-VPC1-2). These first two Varimax-rotated modes are almost identical to Empirical Orthogonal Function (EOF) 1 and EOF 2 presented by *Vuille et al.* [2000] and by *Enfield and Mayer* [1997], although the order between the first and the second EOF is reversed in the latter analysis. ATL-VPC3-6 (not shown) explain a relative small fraction of the total variance (Table 1) and were, as their counterparts in the tropical Pacific, not used any further in this study.

Atlantic SST are not truly independent of the Pacific modes of SST variability. El Niño-related warm (or cold) anomalies similar to the tropical Pacific occur in the Atlantic, although with a lower amplitude and a 4-5 month lag [*Enfield and Mayer*, 1997]. This ENSO influence on SSTs in the tropical Atlantic is best devel-

Table 1. Eigenvalues and Percentage of Total and Cumulative Explained Variance for UPC1 and VPC1-6 Based on the Principal Component Analysis of Tropical Pacific (PAC) and Atlantic (ATL) SSTA

Principal Component	Eigenvalue	Total Explained Variance (%)	Cumulative Explained Variance (%)
PAC-UPC1	69.57	30.78	-
ATL-UPC1	67.89	25.81	-
PAC-VPC1	47.42	20.98	20.98
PAC-VPC2	25.97	11.49	32.47
PAC-VPC3	20.36	9.01	41.48
PAC-VPC4	16.49	7.30	48.78
PAC-VPC5	15.83	7.00	55.78
PAC-VPC6	14.38	6.36	62.14
ATL-VPC1	52.11	19.82	19.82
ATL-VPC2	37.84	14 39	34.21
ATL-VPC3	36.55	13.90	48.11
ATL-VPC4	27.28	10.37	58.48
ATL-VPC5	18.90	7.19	65.67
ATL-VPC6	14.92	5.67	71.34

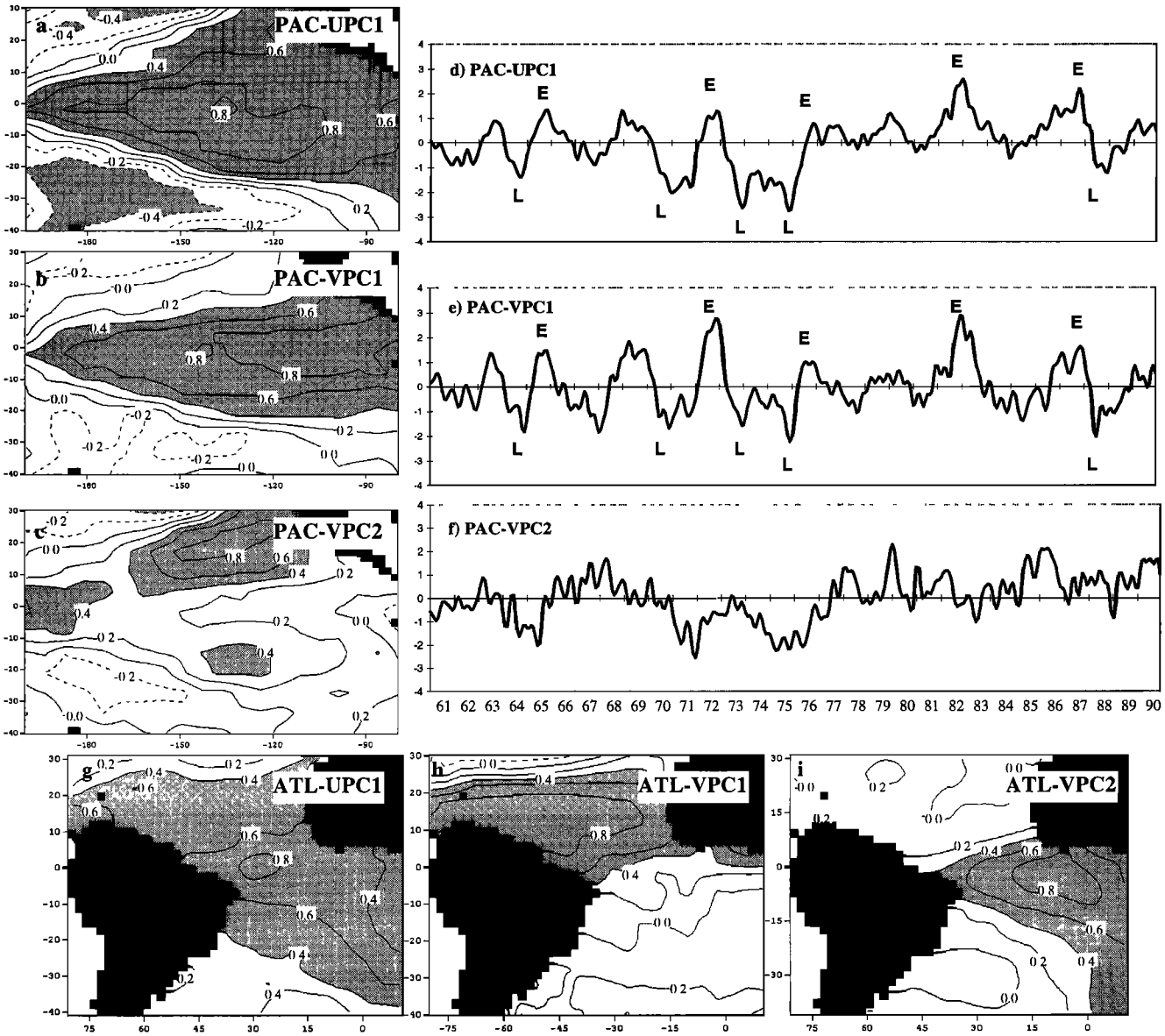

Figure 3. (a) Loading pattern of tropical Pacific SSTA principal component 1 (PAC-UPC1) with contour interval 0.2, values > 0.4 and < -0.4 shaded and negative contours dashed. (b) As in Figure 3a but for PAC-VPC1. (c) As in Figure 3a but for PAC-VPC2. (d) Score time series of PAC-UPC1 with E and L indicating El Niño (E) and La Niña (L) events. (e) As in Figure 3d but for PAC-VPC1. (f) As in Figure 3d but for PAC-VPC2. (g) As in Figure 3a but for ATL-UPC1. (h) As in Figure 3a but for ATL-VPC1. (i) As in Figure 3a but for ATL-VPC2.

oped over the tropical North Atlantic in the area of the NE trades (ATL-VPC1 domain). According to *Enfield and Mayer* [1997] about 50-80% of the anomalous SST variability in this region is associated with ENSO, with Atlantic warmings occurring 4-5 months after the mature phase of Pacific warm events during boreal spring (MAM). These tropical North Atlantic warmings are due to ENSO-induced reductions in surface wind speed within the NE trades through an atmospheric bridge, which lowers the rates of latent and sensible heat loss from the oceanic surface layer [*Curtis and Hastenrath*, 1995; *Enfield and Mayer*, 1997]. These events are important when considering precipitation anomalies over the tropical South American continent, because they are associated with a northward shift in the latitude of the ITCZ and a significant relaxation of the NE trades, which in turn are responsible for furnishing water vapor to the continent and represent a main feature of the summer monsoon system that develops in austral summer over the Altiplano [*Zhou and Lau*, 1998]. *Enfield and Mayer* [1997] even argued that some of the ENSO-related climatic anomalies observed over tropical South America might, in fact, be due to tropical Atlantic SSTA rather than a direct ENSO signal.

4. SSTA Relation to Air Temperature

The basic statistics of the PCA of temperature anomalies over the Central Andes are given in Table 2. Only two PCs were identified as describing significant, nonrandom temperature variability and subsequently rotated using the Varimax criterion (T-VPC1-2). The fact that only two significant eigenvectors emerged from this analysis is not surprising, since it is based on data from

Table 2. Eigenvalues and Percentage of Total and Cumulative Explained Variance of Varimax Rotated Principal Components (VPCs) of Monthly Temperature Anomalies (T) and Summer (DJF) Precipitation

Principal Component	Eigenvalue	Total Explained Variance (%)	Cumulative Explained Variance (%)
T-VPC1	3.25	29.55	29.55
T-VPC2	3.23	29.39	58.94
DJF-VPC1	9.63	31.05	31.05
DJF-VPC2	5.39	17.37	48.42
DJF-VPC3	5.02	16.18	64.60

only 11 stations and the spatial variability of air temperature anomalies over the Altiplano is not very large. The spatial loading patterns and the time evolution of T-VPC1 and T-VPC2 are shown in Figures 4a-4b and 4d-4e, respectively.

T-VPC1 (Figure 4a), explaining 29.6% total variance, is clearly related to ENSO as can be seen from both its temporal evolution (Figure 4d) and its spatial correlation with tropical SSTA (Figure 4f). T-VPC1 shows a pattern of significant positive correlations (95% level), extending from the tropical NE Atlantic westward over the equatorial tropical Pacific toward the dateline. The highest correlation is achieved with a 2-month lag between T-VPC1 and PAC-VPC1; that is, SSTA leads the temperature

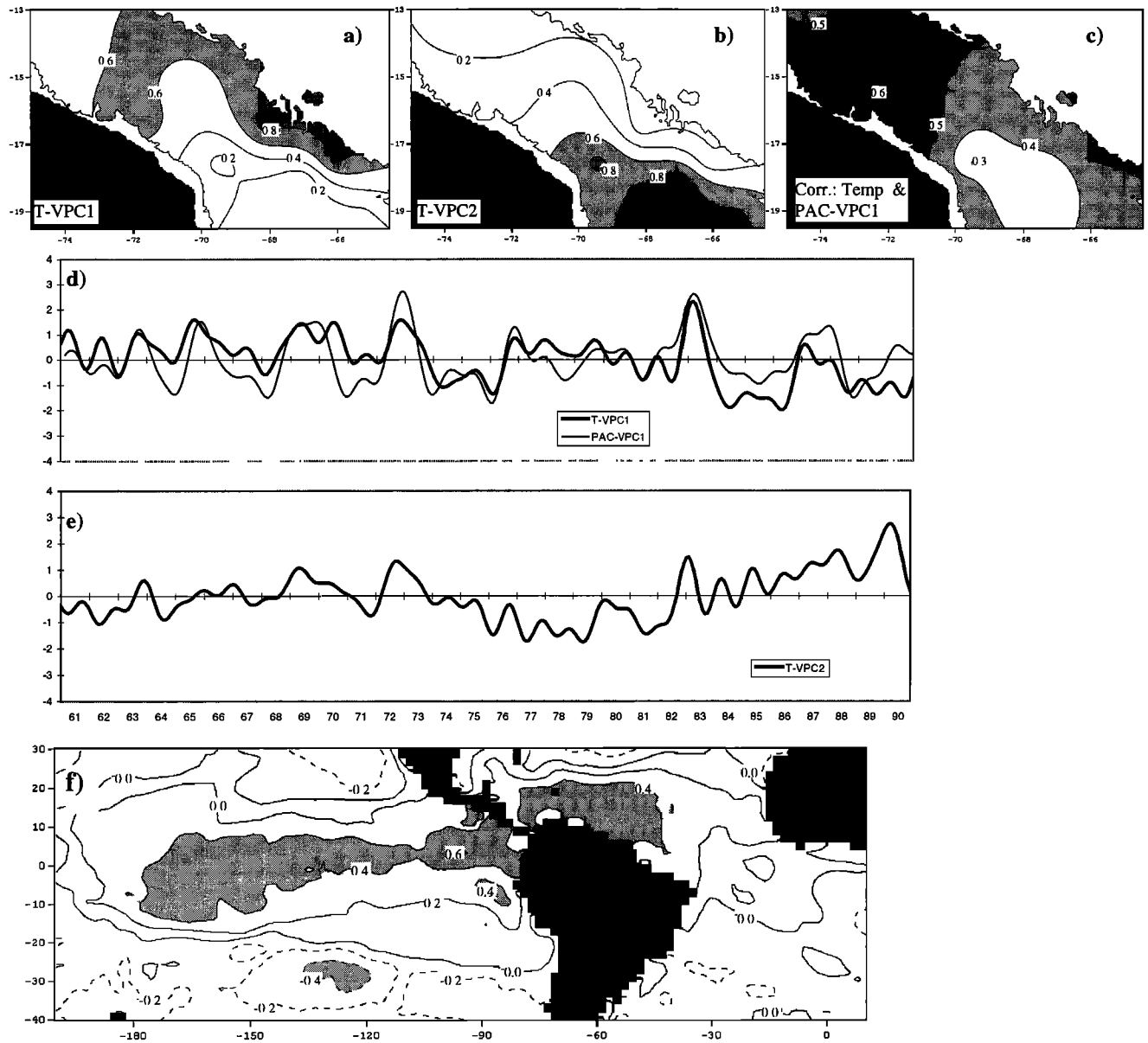

Figure 4. (a) Loading pattern of T-VPC1 with contour interval 0.2, values > 0.6 (0.8) light (dark) shaded. (b) As in Figure 4a but for T-VPC2. (c) Correlation pattern of air temperature anomalies with PAC-VPC1 (2-month lag), with contour intervals of 0.1, and correlation coefficients larger than 0.4 and 0.5 (significant at 95% and 99% levels) light and dark shaded. For all figures only data from areas > 1500 m are plotted (delimited by contour lines). (d) Score time series of T-VPC1 and PAC-VPC1. Both time series are low-pass filtered, retaining periodicities greater than 12 months. PAC-VPC1 leads T-VPC1 by two months. (e) As in Figure 4d but for T-VPC2 only. (f) Pixel-based correlation of tropical Pacific and Atlantic SSTA with score time series of T-VPC1 (lagged by 2 months). Contour interval is 0.2, negative contours are dashed, and values > 0.4 and < -0.4 (significant at 95% level) are shaded.

signal by approximately 2 months (r = 0.58 with PAC-VPC1, significant at 99% level). Correlations with the Southern Oscillation Index (SOI), known to be related to surface and upper air temperature anomalies over the Altiplano [*Aceituno*, 1988, 1989; *Vuille*, 1999] yielded a considerably less significant result (r = -0.45 with a 2-month lag). The spatial loading pattern of T-VPC1 (Figure 4a), shows highest loading along the NE slopes of the Altiplano and a decreasing influence toward the south. This pattern is partially confirmed by the reverse procedure, correlating the Pacific ENSO-mode PAC-VPC1 with temperature station data (Figure 4c). Clearly, the ENSO influence on temperature is less significant over the interior part of the southern Altiplano, but otherwise it shows little differences.

While T-VPC1 is most dominant over the NE part of the Altiplano, T-VPC2, explaining 29.4% of the total variance, shows strongest loadings in the southern Altiplano, south of 18°S (Figure 4d). This mode is associated with a noticeable temperature increase since the late 1970s (Figure 4e), consistent with similar trends observed in the lowlands of northernmost Chile but in strong contrast to the observed cooling trend on the eastern slopes of northwestern Argentina [*Rosenblüth et al.*, 1997]. The correlation of this mode with tropical SSTA (not shown) points toward the tropical South Atlantic, where a similar warming trend has been observed. However, the remote location of the tropical South Atlantic as compared to the tropical Pacific and the fact that the amplitude of tropical Atlantic SSTA is considerably smaller than in the tropical Pacific argue against an Atlantic influence. Also a composite analysis during extreme WARM and COLD periods in the tropical South Atlantic (not shown) yielded clear evidence that the Atlantic influence is limited to southeastern subtropical South America and does not extend toward the Altiplano. The Pacific influence however is very obvious, both based on 600 hPa temperature (~ Altiplano surface level) and station data composites. Temperatures over the Altiplano (600 hPa) are approximately 0.7°-1°C higher two months after PAC-VPC1 WARM events when compared to COLD events in the same domain (Figure 5a). The difference in surface temperature based on station data even amounts to 0.7°-1.3°C (Figure 5b). Again the statistical significance and the temperature difference are higher over the northern part of the Altiplano and decrease toward the south, confirming the patterns in Figures 4a and 4c. These results are in accordance with findings by *Aceituno* [1988, 1989], *Rosenblüth et al.* [1997], and *Vuille* [1999], who showed that significant positive (negative) temperature departures occur at the surface and in the middle troposphere over the Altiplano and northernmost Chile during El Niño (La Niña) events.

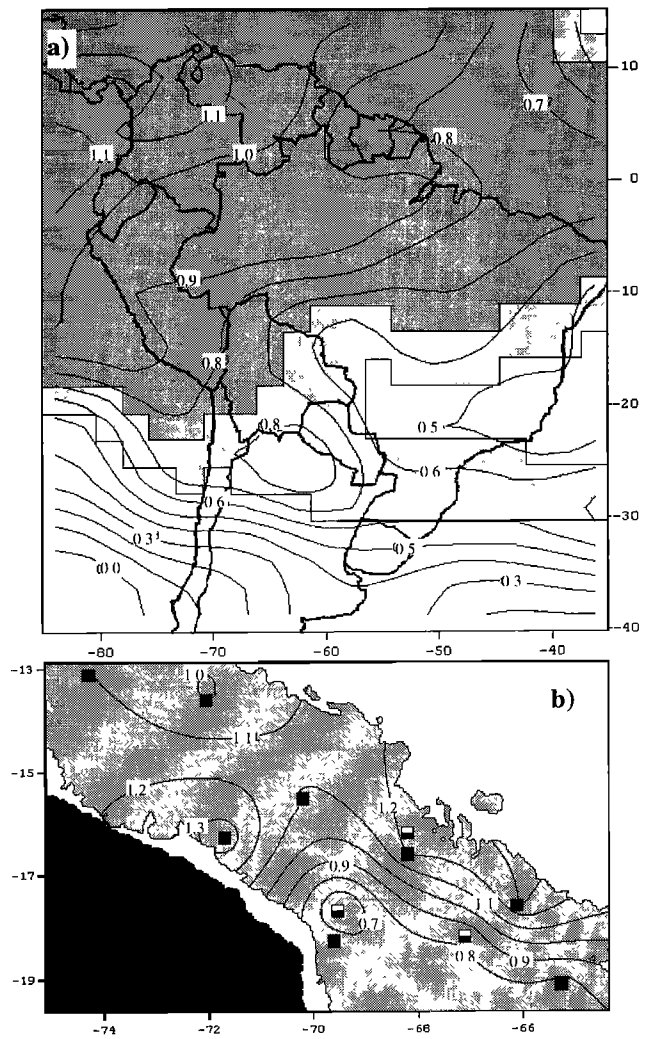

Figure 5. (a) 600 hPa NCEP/NCAR temperature anomaly composite (WARM-COLD) based on score time series of PAC-VPC1. Contour interval is 0.1°C, light (dark) shading indicates significant difference at a 95% (99%) level based on one-sided Student's t-test. PAC-VPC1 WARM periods (score >1) include June - September 1963, July - December 1965, January 1969 - January 1970, May 1972 - March 1973, October - November 1976, August 1982 - August 1983, November 1986 - March 1987, August 1987 - January 1988. PAC-VPC1 COLD periods (score < -1) include October 1964 - January 1965, October 1967-April 1968, August 1970 - March 1971, September - November 1971, October 1973 - February 1974, September 1975 - February 1976, May - August 1985, May - September 1988, January - March 1989. (b) Altiplano station temperature anomaly composite (WARM - COLD) based on score time series of PAC-VPC1 (as in Figure 5a). Contour interval is 0.1; solid (semisolid) squares indicate significant station temperature difference at a 99% (95%) level based on one-sided Students t-test.

5. SSTA Relation to DJF Precipitation

Table 2 also shows the basic statistics of the PCA of DJF precipitation, based on station data from the Central Andes. Note that the region covered by this analysis (11.5°S-20.5°S and 77.5°W-64.5°W) is larger than for the temperature analysis described in the previous section. Three eigenvectors (DJF-VPC1-3) emerged as bearing significant, nonrandom information and were subsequently rotated and further analyzed. The spatial loading patterns of the three modes of austral summer precipitation are shown in Figures 6a-6c, their score time series in Figures 7a-7c and the correlation of their scores with December SSTA in Figures 7d-7e (for DJF-VPC1-2 only). The three eigenvectors show a distinct spatial separation with DJF-VPC1 explaining the highest fraction of the total variance in the more humid eastern Altiplano (Figure 6a), while DJF-VPC2 is the dominant mode in the dry western Altiplano (Figure 6b) and DJF-VPC3 represents summer precipitation variability to the north of the Altiplano in the southern Peruvian Andes between 11.5°S and 15°S (Figure 6c).

DJF-VPC1 explaining 31.1% of the total domain variance is influenced by tropical Pacific SSTA, as can be seen from both its score time series (Figure 7a) and the correlation with contemporaneous SSTA (Figure 7d). The negative correlation with SSTA in the eastern tropical Pacific (significant at the 95% level) suggests that El Niño (La Niña) periods are associated with below (above) average precipitation. However, the relationship is rather

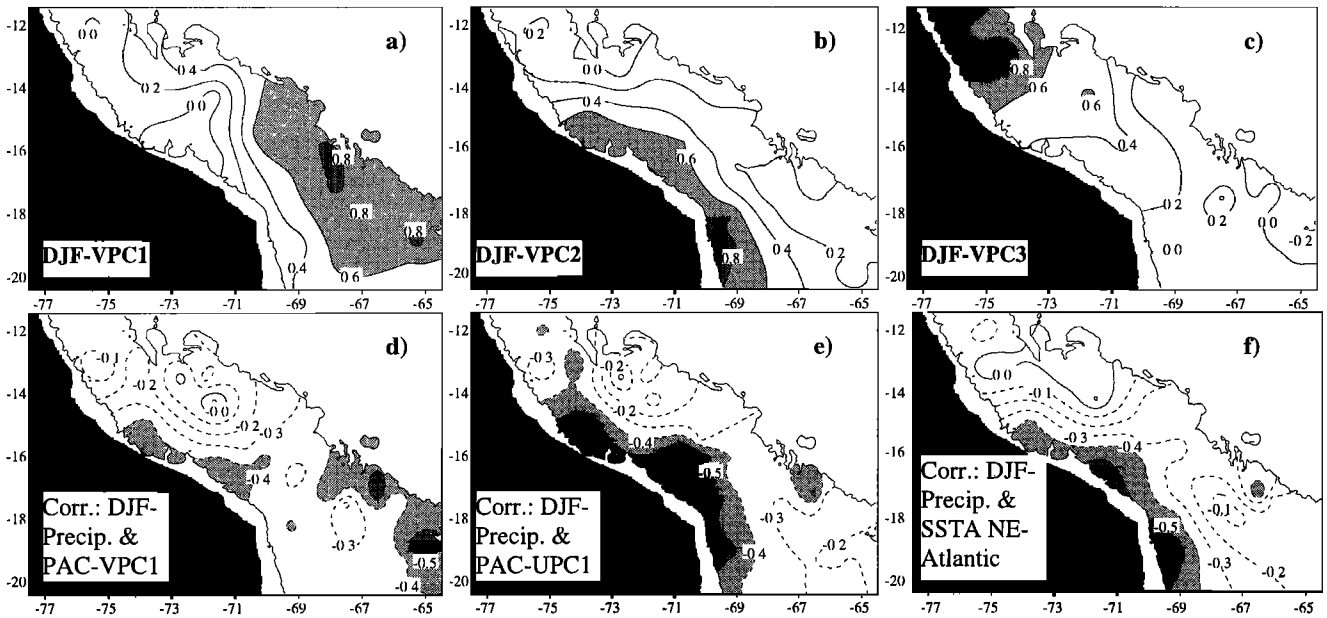

Figure 6. (a) Loading pattern of DJF-VPC1 with contour interval 0.2, values > 0.6 (0.8) shaded light (dark). (b) As in Figure 6a but for DJF-VPC2. (c) As in Figure 6a but for DJF-VPC3. (d) Correlation pattern of DJF precipitation with December score of PAC-VPC1, with contour intervals of 0.1, negative contours dashed, and correlation coefficients < -0.4, and < -0.5 (significant at 95% and 99% levels) light and dark shaded. (e) As in Figure 6d but for correlation with PAC-UPC1. (f) As in Figure 6d but for correlation with SSTA in NE Atlantic (26°N-18°N / 24°W-14°W; see box in Figure 7e). For all figures, only data from areas > 1500 m are plotted (delimited by contour lines). Note that region covered by this analysis is larger than for temperature.

weak; only a limited area in the eastern part of the basin exhibits significant correlations with DJF-VPC1 (Figure 7d). Inspection of the score time series (Figure 7a) confirms this general notion, showing that most El Niño events (E) feature negative scores, while most La Niña events (L) are associated with positive scores. However, this relationship is disturbed after 1986/1987, which was a humid summer, despite the warm conditions in the tropical Pacific. On the other hand, later, during the La Niña summer 1988/1989, the eastern Altiplano received below average precipitation (Figure 7a). The area in the tropical Pacific featuring highest correlations with DJF-VPC1 is best represented by mode PAC-VPC1 (see Figure 3b). Accordingly, the reverse procedure was applied to test the significance of these results, by correlating the December scores of PAC-VPC1 with DJF station precipitation data. The result, shown in Figure 6d, indeed compares favorably with the spatial loading pattern of DJF-VPC1 (Figure 6a), thereby confirming the influence of eastern tropical Pacific SSTA on the eastern flanks of the Altiplano. However, the affected area seems to be considerably smaller than assumed from the previous analysis. Significant correlations (a correlation of 0.37 (0.47) is statistically significant at the 95% (99%) level) also emerge over the dry western slopes of southern Peru, not primarily related to DJF-VPC1.

The comparison of the score time series of DJF-VPC2 with the El Niño and La Niña periods that occurred over this 30-year period does not seem to support the notion of a strong ENSO influence on summer precipitation in this part of the Altiplano (Figure 7b). However, correlations of DJF-VPC2 with contemporaneous SSTA are significant over almost the entire tropical Pacific and even feature the typical ENSO-tongue with positive correlations in the southwestern and northwestern part of the basin (Figure 7e). The entire correlation pattern matches surprisingly well with the spatial loading pattern of PAC-UPC1 (compare Figure 7e with PAC-UPC1 in Figure 3a), yielding clear evidence for a strong tropical Pacific influence over the dry western Altiplano. It is noteworthy that the strongest (positive) correlations emerge over the South Pacific Convergence Zone (SPCZ) region in the subtropical South Pacific. This is consistent with similar results obtained by *Lenters and Cook* [1999], who argued that the link between interannual precipitation variability on the Altiplano and ENSO may be through the SPCZ, which usually is displaced eastward during El Niño and shows clear teleconnection patterns with convective activity over the subtropical part of the continent. The increased frontal activity in eastern South America may in turn lead to dry and convectively unfavorable conditions over the Altiplano [*Lenters and Cook,* 1999]. The score time series of DJF-VPC2 exhibits a strong decadal-scale oscillation with above-average precipitation from the late 1960s to the mid 1970s followed by a decade of dry conditions in the late 1970s and 1980s (Figure 7b). Given the relationship with tropical Pacific SSTA, it is very probable that this decadal-scale precipitation variability is related to the contemporaneous climatic shift in the tropical Pacific domain in the late 1970s [*Ebbesmeyer* et al., 1991]. Apparently, the ENSO relationship over the western Altiplano is modulated by a decadal mode of Pacific SSTA variability, which would explain the unexpected dry La Niña summer 1964/1965 or the humid El Niño summers 1972/1973 and 1976/1977. Another explanation for these exceptions is that ENSO may peak early (as in 1976) or late in the season and the influence on DJF rainfall therefore varies from one event to the next. Another region of significant negative correlations in Figure 7e emerges off the coast of NW Africa in the northeastern part of the tropical North Atlantic. This relationship suggests that cold (warm) SSTA in the tropical North Atlantic might be related to an increase (decrease)

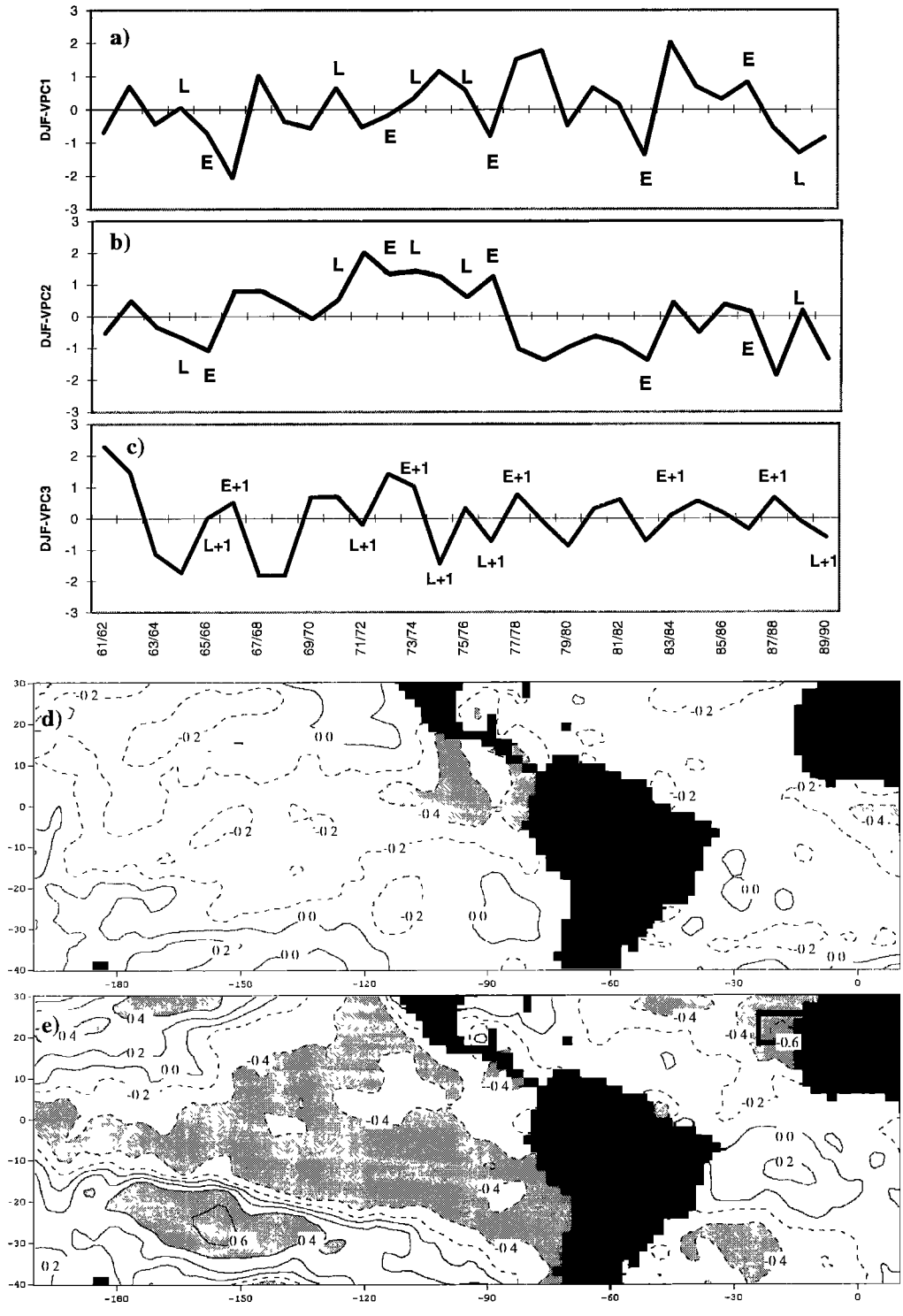

Figure 7. (a) Score time series of DJF-VPC1 with E and L indicating El Niño (E) and La Niña (L) events. (b) As in Figure 7a but for DJF-VPC2. (c) As in Figure 7a but for DJF-VPC3 and E+1 (L+1) indicating year following an El Niño (La Niña) event. (d) Pixel-based correlation of tropical Pacific and Atlantic SSTA in December with score time series of DJF-VPC1. Contour interval is 0.2, negative contours are dashed, and values > 0.4 and < -0.4 (significant at 95% level) are shaded. (e) As in Figure 7d but for DJF-VPC2. Black box (26°N-18°N / 24°W-14°W) indicates SSTA region in NE Atlantic used for correlation with DJF precipitation in Figures 6f and 9a.

in precipitation over the western Altiplano. A third coherent region of negative correlations is located over the tropical South Atlantic. While this latter correlation pattern could not be confirmed by the reverse analysis, the December scores of PAC-UPC1 and SSTA off the coast of NW Africa (26°N-18°N / 24°W-14°W; see box in Figure 7e) are both significantly correlated with DJF station precipitation. The correlation patterns in Figure 6e (PAC-UPC1) and Figure 6f (NE Atlantic SSTA) resemble the loading pattern of DJF-VPC2 in a striking manner, featuring a clear east-west gradient across the Altiplano, with the signifi-

cance of the correlation increasing toward the west. It is noteworthy that the significant negative correlations in the northeastern tropical Atlantic occur exactly where the NE trades emanate from the Sahara High, thereby representing a main feature of the South American summer monsoon system [*Zhou and Lau,* 1998].

DJF-VPC3, explaining 16.2% of the total domain variance, is the dominant mode in the northernmost part of the study area in southern Peru (Figure 6c). Significant pixel-based cross correlations of the score time series with contemporaneous SSTA (not shown) are confined to small areas over the southeastern tropical Pacific, not directly related to ENSO. The inspection of the score time series of DJF-VPC3 (Figure 7c), however, yields a remarkable result, featuring a reversal of the ENSO signal in the following year. Above-average precipitation occurs in the year following an El Niño event (E+1), while years following a La Niña event (L+1) are consistently drier than normal.

6. Discussion

Several of the observations made in section 5 are interesting and deserve further investigation: Why is the ENSO signal stronger over the western than over the eastern Altiplano (compare Figures 6a-6b with 7d-7e)? Is precipitation over the western Altiplano (DJF-VPC2) indeed related to SSTA in the tropical NE Atlantic? How can the delayed ENSO signal in the DJF-VPC3 domain be explained?

In search for an answer for the first question, we analyzed composites of several meteorological fields during periods of extreme oceanic forcing in the PAC-UPC1 domain, which is most closely related to precipitation variability over the western Altiplano. In Figure 8 we present DJF composites of 200 hPa geopotential height and wind (Figure 8a), OLR (Figure 8b) and Altiplano precipitation (Figure 8c). All composites represent the difference between the six strongest (four for OLR) COLD and WARM events (mean DJF SSTA) in the PAC-UPC1 domain.

Clearly, the upper air circulation over the Altiplano is significantly altered (99% level) during ENSO conditions in the Pacific (Figure 8a). During austral summer, Pacific COLD (WARM) events are characterized by a largely reduced (increased) geopotential height over tropical South America and only weak negative (positive) departures in the subtropical part of the continent, thereby leading to a reduced (enhanced) meridional height gradient and easterly (westerly) wind anomalies over the Altiplano at the 200 hPa level. This is consistent with observations made by *Aceituno* [1989] and has been linked to the observed increase (decrease) in DJF precipitation during La Niña (El Niño) periods [*Vuille,* 1999]. Although no moisture is advected toward the Altiplano at the 200 hPa level, upper air easterly winds are responsible for a turbulent entrainment of lower-level winds over the eastern Andean ridge, which in turn lead to an upslope flow of moist air from the east toward the Altiplano [*Garreaud,* 1999]. This moisture flux at the 500 hPa and lower levels, however, is hard to monitor with reanalysis data due to its poor resolution in comparison with the Andean topography. While the 500 hPa DJF zonal wind anomalies are significantly different between El Niño and La Niña episodes in radiosonde data from La Paz, this is not the case in the reanalysis data [see *Vuille,* 1999]. The 200 hPa wind pattern is therefore more suitable to describe the anomalous circulation during COLD and WARM events. While the prevailing easterly wind anomalies during COLD (La Niña) conditions are very favorable for precipitation over the western part of the Altiplano, westerly wind anomalies inhibit moisture advection from the east during El Niño (WARM) periods. Thus convection can still occur over the eastern Altiplano slopes under such circumstances, but the western part of the Altiplano remains dry [*Garreaud,* 1999]. Accordingly the western Altiplano is much more sensitive to such ENSO-induced atmospheric circulation anomalies. The large-scale DJF precipitation pattern based on OLR data (Figure 8b) does not yield much further insight into this mechanism. Although OLR is reduced during COLD as compared to WARM over the southwestern part of the Altiplano, the difference is only ~5 W m^{-2} and not significant at the 95% level. Obviously the coarse resolution (2.5° × 2.5°) and the short time period covered by the data (1974-1990) is not suitable to distinguish the differences in convective activity and precipitation across the Altiplano. A better resolved pattern emerges from the composite based on Altiplano precipitation data (Figure 8c). While precipitation over the eastern and northern part of the Altiplano is less than 25% higher during COLD as compared to WARM events, the difference is much larger toward the west, reaching more than 100% along the western margin of the Altiplano. Clearly, the dry western Altiplano is much more sensitive to such ENSO-induced precipitation anomalies than the east.

The highly significant negative correlation between austral summer precipitation over the western Altiplano and SSTA in the NE-Atlantic (Figures 6f and 7e) is another interesting issue that deserves further investigation. It is well established how cold (warm) SSTA in the tropical North Atlantic can lead to increased (decreased) precipitation over NE Brazil [e.g., *Mechoso et al.,* 1990], the southern Amazon Basin [*Marengo and Hastenrath,* 1993], and even the eastern Andean slopes of Ecuador [*Vuille et al.,* 2000], especially if contemporaneous warm anomalies occur south of the equator, thereby leading to a southward displacement of the ITCZ toward the warmer waters. Unlike these regions however, the Altiplano is not under a direct influence of the trade wind system. Moisture flux toward the dry western part of the Altiplano is coupled with intensified middle and upper tropospheric easterlies, usually associated with a strengthened and southward displaced Bolivian High. The strong summer convection over the Altiplano on the other hand may be a precursor of SSTs off the coast of NW Africa through an upper air monsoon-type return flow and a modification of the strength of the NE trade winds emanating from the Sahara High [*Zhou and Lau,* 1998]. Time-lagged correlation analysis between Altiplano precipitation (DJF-VPC2) and raw SSTA off the coast of NW Africa (26°N-18°N / 24°W-14°W), smoothed with a 3-month running mean, reveals that Altiplano precipitation indeed leads SSTA in the NE Atlantic. Although the correlation is significant at lag 0 (r = -0.50, significant at 99% level), highest correlations (r = -0.64, significant at 99.9% level) are achieved when Altiplano precipitation (DJF-VPC2) leads SSTA off the coast of NW Africa by approximately 2-3 months (Figure 9a). This is consistent with results by *Nobre and Shukla* [1996], who found a similar 2-month lag between strongest wind stress anomalies and maximum SSTA over the NE tropical Atlantic off the coast of NW Africa. Composite analysis of tropical Atlantic SSTA in March further confirms this notion (Figures 9c-9d). While Figure 9c represents the average SSTA in March following the five most humid summers over the western Altiplano (DJF-VPC2 domain), Figure 9d shows the opposite pattern (March SSTA following the five driest summers). Clearly below (above) average SSTs emerge in March (2-month lag) after strong (weak) convective activity over the Altiplano region. Although further investigation on this issue is warranted, tropical heating and convection over

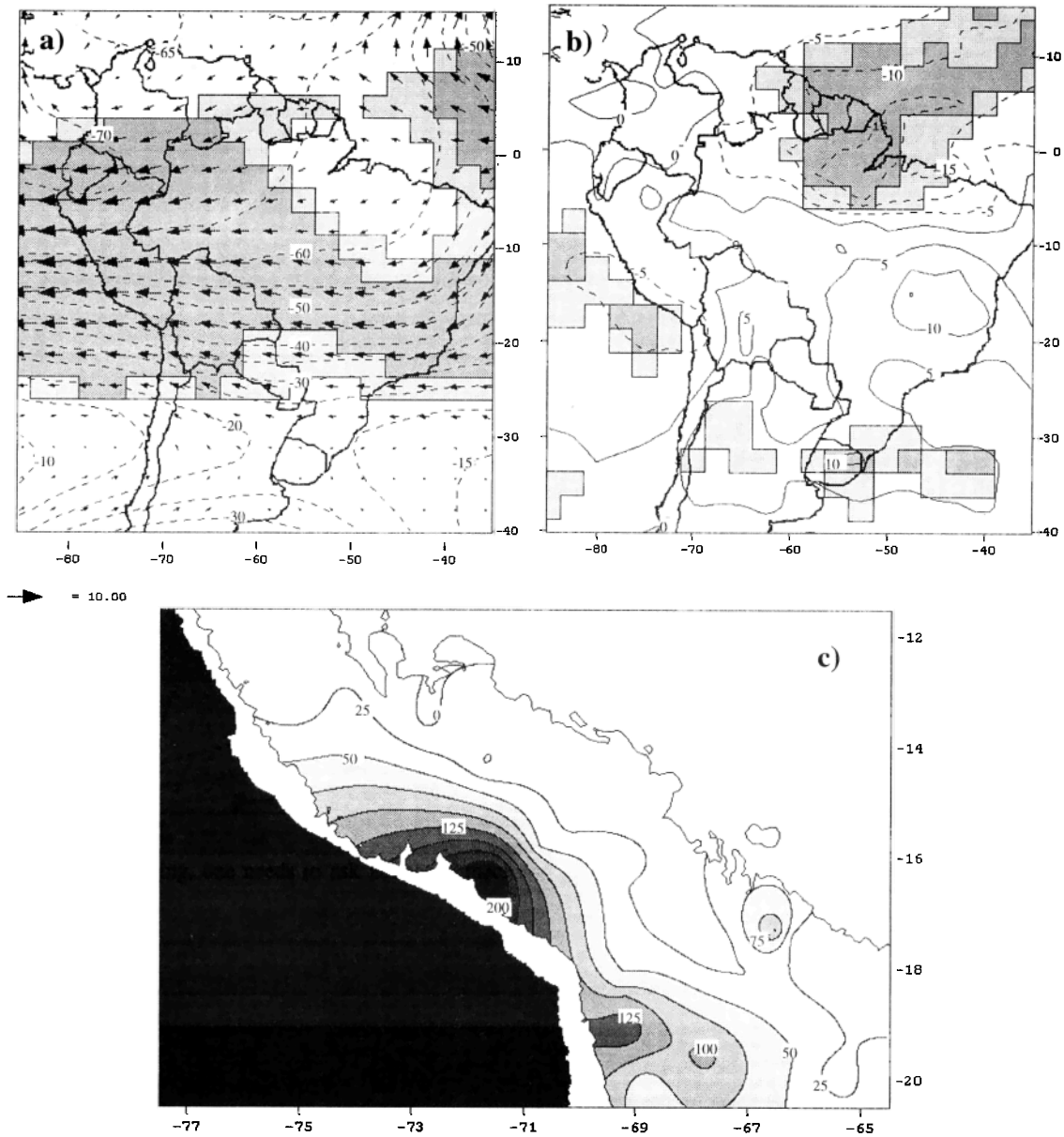

Figure 8. (a) NCEP/NCAR 200 hPa DJF wind and geopotential height difference composite (COLD-WARM) based on six warmest and coldest DJF scores of PAC-UPC1. COLD periods include 1970/1971, 1971/1972, 1973/1974, 1974/1975, 1975/1976, and 1988/1989; WARM composite is based on 1968/1969, 1972/1973, 1979/1980, 1982/1983, 1986/1987, and 1987/1988. Contour interval is 5 gpm, negative values are dashed, and light (dark) shading indicates significant zonal wind anomalies at 95% (99%) level based on two-tailed Student's *t*-test. (b) As in Figure 8a but for OLR. COLD periods include 1974/1975, 1975/1976, 1984/1985, and 1988/1989; WARM periods include 1979/1980, 1982/1983, 1986/1987, and 1987/1988. Contour interval is 5 W m^{-2}; negative contours are dashed. (c) As in Figure 8a but for DJF Altiplano precipitation (precipitation excess (in %) during COLD as compared to WARM). Contour interval is 25%, values above 50% are indicated by gray shading.

the Altiplano certainly has the potential to considerably alter SSTs off NW-Africa through anomalous NE trades, emanating from the Sahara High.

Finally, the ENSO signal in the DJF-VPC3 domain, apparently reversed and delayed by a year (Figure 7c) is an issue that deserves investigation. Lagged correlation analysis reveals that DJF-VPC3 and PAC-VPC1 are not significantly correlated at lag zero, but significant positive correlations (95% level) appear when an 8- to 12-month lag is introduced (Figure 9b). Since atmospheric circulation anomalies usually occur as an immediate response to oceanic forcing, one needs to ask about the mechanisms involved. The phenomenon has been observed in previous studies [*Ronchail*, 1995; *Vuille*, 1999], but a clear answer for its origin is lacking. One possible explanation for a delayed ENSO signal over tropical South America is related to a transfer of the signal into the tropical North Atlantic. However, we could not find significant correlations between DJF-VPC3 and tropical North Atlantic SSTA at any lags. Furthermore the ENSO signal appears strongest in the tropical North Atlantic in boreal spring (MAM) [*Curtis and Hastenrath*, 1995; *Enfield and Mayer*, 1997], too late to have an impact on austral summer precipitation (DJF) and is of the same sign as in the tropical Pacific, which

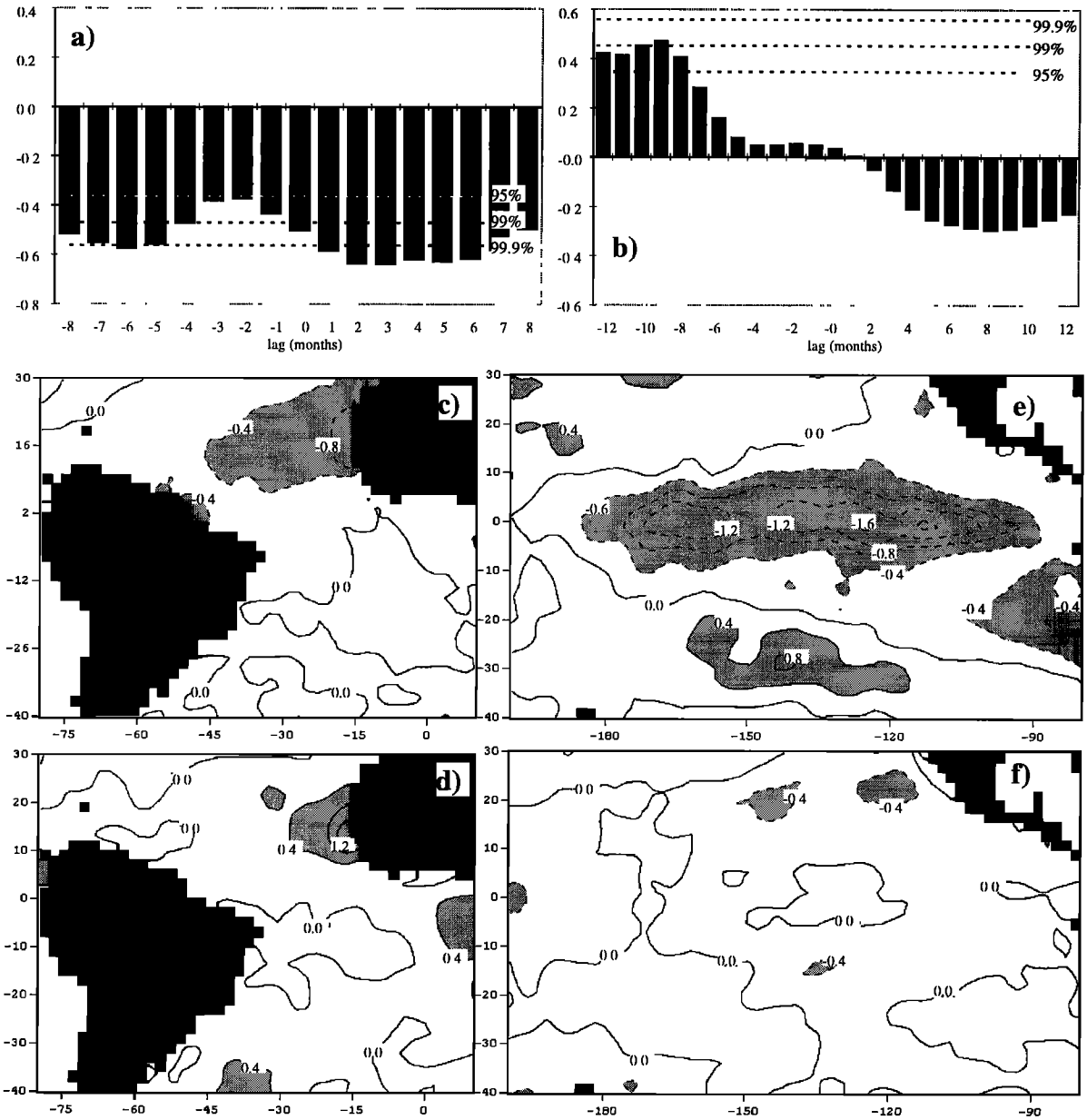

Figure 9. (a) Time-lagged correlation coefficients between score time series of DJF-VPC2 and SSTA in tropical NE Atlantic (26°N-18°N / 24°W-14°W). Positive (negative) lag indicates that DJF-VPC2 leads (lags) Atlantic SSTA. SSTA time series is smoothed with a 3-month running mean. (b) As in Figure 9a but for correlation between score time series of DJF-VPC3 and PAC-VPC1. (c) Tropical Atlantic SSTA composite in March following five most humid DJF rainy seasons in the western Altiplano (1972, 1973, 1974, 1975, and 1977). Contour interval is 0.4°C, negative contours are dashed, and values > 0.4°C and < -0.4°C are shaded. (d) As in Figure 9c but for March following five driest DJF seasons (1966, 1979, 1983, 1988, and 1990). (e) Tropical Pacific SSTA composite in December following five strongest El Niño events (8-12 months after peak of PAC-VPC1 score; 1966, 1970, 1973, 1983, and 1988). (f) As in Figure 9e but for December following five strongest La Niña events (1965, 1968, 1971, 1976, and 1989).

makes such a relationship even more unlikely. Rather than a delayed signal, we presume it is related to the fact that SSTAs in the tropical Pacific often switch from one extreme phase to its opposite within a year (e.g., La Niña 1964/1965 was followed by El Niño 1965/1966, El Niño 1972/1973 was followed by La Niña 1973/1974, La Niña 1975/1976 was followed by El Niño 1976/1977). Figures 9e-9f show December SSTA composites in the tropical Pacific approximately 1 year (within 8-12 months after the SSTA peak) after the five strongest El Niño (La Niña) events (based on the peak values of the score time series of PAC-VPC1). On average, one year after the peak phase of El Niño conditions, SSTA in the tropical Pacific have completely reversed and feature negative anomalies, which resemble typical La Niña conditions (Figure 9e). The opposite pattern however, does not usually occur. One year after the peak phase of La Niña events, SSTA in the tropical Pacific are close to average and do not show any sign of an evolving El Niño event (Figure 9f). This notion is also confirmed by a closer inspection of the score time series of

PAC-VPC1 (see Figure 3e). While SSTs usually drop dramatically after the peak phase of an El Niño event has been reached, recovery from below-average SSTA (La Niña events) is much slower, which explains why austral summers following an El Niño event (E+1) feature above-average precipitation, yet the dry conditions following a La Niña event are less pronounced [see *Vuille*, 1999]. This biennial tendency of ENSO is a feature noted before [*Kiladis and Diaz*, 1989] and offers some potential for prediction of austral summer precipitation in the DJF-VPC3 domain.

7. Summary and Conclusions

The purpose of this study was to identify the main spatiotemporal modes of temperature and austral summer (DJF) precipitation variability in the Central Andes, based on a two-way PCA and composite analysis.

Because of the closer proximity to the Pacific and the much larger amplitude of SSTA in this basin, temperature variability in the Central Andes is primarily related to ENSO. The spatial pattern of temperature variability is quite uniform and responds to Pacific SSTA in the central equatorial Pacific with a lag of approximately 1-2 months. Temperature closely follows SSTA in the NINO3 and NINO4 domain. The second temperature mode, dominant over the southern Altiplano (T-VPC2) features a significant increase in temperature starting in the late 70s.

Precipitation variability in austral summer (DJF) is also primarily related to SSTA in the tropical Pacific domain. The ENSO signal however is modified in the different parts of the Altiplano, although the general pattern of below (above) average precipitation during El Niño (La Niña) conditions remains the same. Over the eastern part of the Altiplano, correlations with ENSO are weak, because El Niño-induced westerly wind disturbances do not modulate convection and precipitation over the eastern Andean slopes. The western part of the Altiplano however, is more sensitive to such ENSO-induced atmospheric circulation anomalies because moisture advection from the east is significantly lowered (increased) during El Niño (La Niña) periods. The interannual precipitation variability over the western part of the Altiplano thus more closely follows SSTA in the tropical Pacific domain and features a clear decadal-scale oscillation with above-average precipitation from the late 1960s to the mid 1970s followed by a decade of dry conditions in the late 1970s and 1980s. This precipitation signal is related to the contemporaneous climatic shift in the tropical Pacific domain in the late 1970s, featuring an increased number of El Niños and less La Niña events. In the northernmost part of the study area a pronounced signal emerges with a delay of 8-12 months (i.e., the austral summer following the peak phase of ENSO). The increase (decrease) in precipitation in the summer following an El Niño (La Niña) event is not a physically delayed signal but rather related to the internal evolution of tropical Pacific SSTA, rapidly switching from one state to the other.

Despite the fact that the moisture source for Central Andean precipitation lies to the east in the continental lowlands and ultimately in the tropical Atlantic, SSTAs in this domain do not have a strong influence on DJF precipitation variability over the Altiplano. On the contrary, during boreal spring (March) SSTAs in the tropical NE Atlantic domain off the coast of NW Africa are considerably influenced by heating and convection over the Altiplano through an upper air monsoon return flow, altering the strength of the NE trades which emanate from the Sahara High.

Several earlier studies have reported on the relationship between interannual variability of summer precipitation in the Central Andes and ENSO. In most of these studies, the relationship was described as rather weak, barely reaching statistical significance. It seems that Pacific SSTA modes extracted by means of PCA yield better results than SSTA averaged over specific regions (NINO indices) or when the SOI is used as a proxy. Even more important, however, is to account for the large spatial precipitation variability over the Altiplano by subdividing the Altiplano into regions of similar and coherent modes of variability. This method has enabled us to show how precipitation variability in the different parts of the Altiplano relates to tropical SSTA, in particular to ENSO.

Acknowledgments. Precipitation and temperature data were obtained from the Dirección General de Aguas in Arica (Chile) and the Instituto Nacional de Recursos Naturales (INRENA) in Lima. Both institutions are gratefully acknowledged. Additional data for Peru was kindly provided by Uwe Dornbusch, Cesar Portocarrero and José Dapozzo, and by Josyanne Ronchail, Sandra Rome-Gaspaldy, Yves Arnaud and Lita Buttolph for Bolivia. Chris Folland and David Parker contributed the GISST data set. Interpolated OLR and NCEP/NCAR reanalysis data were provided by NOAA-CIRES Climate Diagnostics Center. Janette Piemonte-Gartner is gratefully acknowledged for her assistance in establishing the precipitation and temperature database. Douglas R. Hardy and anonymous reviewers provided valuable comments that helped to improve considerably this manuscript This study was financed by US-NSF (grant ATM 9707698) and Swiss NSF (grant 8220-050401). Both agencies are gratefully acknowledged.

References

Aceituno, P , On the functioning of the Southern Oscillation in the South American sector, part I; Surface climate, *Mon Weather Rev, 116*, 505-524, 1988

Aceituno, P , On the functioning of the Southern Oscillation in the South American sector, part II; Upper-air circulation, *J. Clim.*, 2, 341-355, 1989.

Aceituno, P , and A. Montecinos, Circulation anomalies associated with dry and wet periods in the South American Altiplano, in *Proceedings of the 4th International Conference on Southern Hemisphere Meteorology*, pp. 330-331, Am. Meteorol. Soc., Boston, Mass., 1993.

Curtis, S., and S. Hastenrath, Forcing of anomalous sea surface temperature evolution in the tropical Atlantic during Pacific warm events, *J Geophys. Res., 100*, 15,835-15,847, 1995.

Davis, R. E., Predictability of sea surface temperature and sea level pressure anomalies over the North Pacific Ocean, *J. Phys. Oceanogr , 6*, 249-266, 1976.

Ebbesmeyer, C. C , D. R., Cayan, D. R., McLain, F. H. Nichols, D. H. Peterson, and K. T. Redmond, 1976 Step in the Pacific climate: Forty environmental changes between 1968-75 and 1977-1984, in *Proceedings of the 7th Annual Pacific Climate (PACLIM) Meeting Workshop*, edited by J. L. Betancourt and V. L. Tharp, *Tech. Rep. 26*, Calif. Dep. of Water Resour., Sacramento, Calif., 1991.

Enfield, D. B., Relationship of inter-American rainfall to tropical Atlantic and Pacific SST variability, *Geophys. Res. Lett., 23* (23), 3305-3308, 1996.

Enfield, D. B., and D. A. Mayer, Tropical Atlantic SST variability and its relation to El Niño-Southern Oscillation, *J. Geophys. Res., 102*, 929-945, 1997.

Garreaud, R. D., Multi-scale analysis of the summertime precipitation over the Central Andes, *Mon. Weather Rev.,127*, 901-921, 1999.

Garreaud, R. D., and J.M. Wallace, The diurnal march of convective cloudiness over the Americas, *Mon. Weather Rev., 125*, 3157-3171, 1997.

Hardy, D. R., M. Vuille, C. Braun, F. Keimig, and R. S. Bradley, Annual and daily meteorological cycles at high altitude on a tropical mountain, *Bull. Am. Meteorol. Soc.,79* (9), 1899-1913, 1998.

Horel, J D , A. N. Hahmann, and J E Geisler, An investigation of the annual cycle of convective activity over the tropical Americas, *J. Clim., 2*, 1388-1403, 1989.

Jacobeit, J., Die grossräumige Höhenströmung in der Hauptregenzeit

feuchter und trockener Jahre über dem südamerikanischen Altiplano, *Meteorol. Z., 6*, 276-284, 1992.

Kalnay, E., et al., The NCEP/NCAR 40-year reanalysis project, *Bull. Am. Meteorol. Soc.*, *77*(3), 437-471, 1996.

Karl, T. R., A. J. Koscielny, and H. F. Diaz, Potential errors in the application of principal component (eigenvector) analysis to geophysical data, *J. Appl. Meteorol.*, *21*, 1183-1186, 1982.

Kiladis, G. N., and H. F. Diaz, Global climatic anomalies associated with extremes in the Southern Oscillation, *J. Clim.*, *2*, 1069-1090, 1989.

Kousky, V. E., and M. T. Kayano, Principal modes of outgoing longwave radiation and 250 mb circulation for the South American sector, *J. Clim.*, *7*, 1131-1143, 1994.

Lenters, J. D., and K. H. Cook, On the origin of the Bolivian High and related circulation features of the South American climate, *J. Atmos. Sci.*, *54*, 656-677, 1997.

Lenters, J. D., and K. H. Cook, Summertime precipitation over South America: Role of the large-scale circulation, *Mon. Weather Rev.*, *127*, 409-431, 1999.

Liebmann, B., and C. A. Smith, Description of a complete (interpolated) outgoing longwave radiation data set, *Bull. Am. Meteorol. Soc.*, *77*(6), 1275-1277, 1996.

Marengo, J. A., and S. Hastenrath, Case studies of extreme climatic events in the Amazon Basin, *J. Clim.*, *6*, 617-627, 1993.

Mechoso, C. R., S. W. Lyons, and J. A. Spahr, The impact of sea surface temperature anomalies on the rainfall over northeast Brazil. *J. Clim.*, *3*, 812-826, 1990.

Montroy, D. L., Linear relation of central and eastern North American precipitation to tropical Pacific sea surface temperature anomalies, *J. Clim.*, *10*, 541-558, 1997.

Nobre, P., and J. Shukla, Variations of sea surface temperature, wind stress, and rainfall over the tropical Atlantic and South America, *J. Clim.*, *9*, 2464-2479, 1996.

North, G. R , T. L. Bell, R. F. Cahalan, and F. J. Moeng, Sampling errors in the estimation of Empirical Orthogonal Functions, *Mon. Weather Rev.*, *110*, 699-706, 1982.

Overland, J. E., and R. W. Preisendorfer, A significance test for Principal Components applied to a cyclone climatology, *Mon. Weather Rev.*, *110*, 1-4, 1982.

Richman, M. B., Rotation of principal components, *J. Climatol.*, *6*, 293-335, 1986.

Richman, M. B., and P. J. Lamb, Climatic pattern analysis of three- and seven-day summer rainfall in the central United States: Some methodological considerations and a regionalization, *J. Clim. Appl. Meteorol.*, *24*, 1325-1343, 1985.

Ronchail, J., Variabilidad interanual de las precipitaciones en Bolivia, *Bull. Inst. Fr. Etud. Andines*, *24*(3), 369-378, 1995.

Rosenblüth, B., H. A. Fuenzalida, and P. Aceituno, Recent temperature variations in southern South America, *Int. J. Climatol.*, *17*, 67-85, 1997.

Silva Dias, P. L., W. H. Schubert, and M. DeMaria, Large-scale response of the tropical atmosphere to transient convection, *J. Atmos. Sci.*, *40*, 2689-2707, 1983.

Stearns, S. D., and R. A. David, Signal processing algorithms, in *Prentice Hall signal processing Series*, edited by A. V. Oppenheim, 349 pp., Prentice-Hall, Englewood Cliffs, N.J., 1988.

Thompson, L. G., E. Mosley-Thompson, and B. J. Arnao, El Niño-Southern Oscillation events recorded in the stratigraphy of the tropical Quelccaya ice cap, Peru, *Science, 226*, 50-52, 1984.

Tourre, Y. M., and W. B. White, ENSO signals in global upper-ocean temperature, *J. Phys. Oceanogr.*, *25*, 1317-1332, 1995.

Vuille, M., Atmospheric circulation anomalies over the Bolivian Altiplano during dry and wet periods and extreme phases of the Southern Oscillation, *Int. J. Climatol.*, *19*, 1579-1600, 1999.

Vuille, M., and C. Ammann, Regional snowfall patterns in the high arid Andes, *Clim. Change*, *36*(3-4), 413-423, 1997.

Vuille, M., D. R. Hardy, C. Braun, F. Keimig, and R. S. Bradley, Atmospheric circulation anomalies associated with 1996/1997 summer precipitation events on Sajama Ice Cap, Bolivia, *J. Geophys. Res.*, *103*, 11,191-11,204, 1998.

Vuille, M., R. S. Bradley, and F. Keimig, Climate variability in the Andes of Ecuador and its relation to tropical Pacific and Atlantic sea surface temperature anomalies, *J. Clim.*, in press, 2000.

Zhou, J., and K.-M. Lau, Does a monsoon climate exist over South America?, *J. Clim.*, *11*, 1020-1040, 1998.

R. S. Bradley, F. Keimig and M. Vuille, Climate System Research Center, Department of Geosciences, Morrill Science Center, University of Massachusetts, Amherst, MA 01003-5820. (rbradley@geo.umass.edu; frank@geo.umass.edu; mathias@geo.umass.edu.)

(Received September 3, 1999; revised January 6, 2000;
accepted February 12, 2000.)